frontiers in Nanotechnology

ORIGINAL RESEARCH
published: 20 May 2021
doi: 10.3389/fnano.2021.684788

Visible-Light-Driven Photocatalytic Water Disinfection Toward *Escherichia coli* by Nanowired g-C_3N_4 Film

Yizhu Zhang[1], *Shigang Su*[1], *Yuanyuan Zhang*[1], *Xia Zhang*[1], *Paolo Giusto*[2]*, *Xiaohua Huang*[3]* and *Jian Liu*[1]*

[1]College of Materials Science and Engineering, Qingdao University of Science and Technology, Qingdao, China, [2]Department of Colloid Chemistry, Max Planck Institute of Colloids and Interfaces, Potsdam, Germany, [3]Bestee Materials (Tsingdao) Co. Ltd., Qingdao, China

OPEN ACCESS

Edited by:
Jesus Barrio,
Imperial College London,
United Kingdom

Reviewed by:
Nailiang Yang,
Institute of Process Engineering (CAS),
China
Kai Xiao,
Leibniz Institute for Solid State and
Materials Research Dresden (IFW
Dresden), Germany

***Correspondence:**
Paolo Giusto
Paolo.Giusto@mpikg.mpg.de
Xiaohua Huang
huangxiaohua@by-herb.com
Jian Liu
mailto:liujian@qust.edu.cnl

Specialty section:
This article was submitted to
Nanotechnology for Energy
Applications,
a section of the journal
Frontiers in Nanotechnology

Received: 24 March 2021
Accepted: 13 April 2021
Published: 20 May 2021

Citation:
Zhang Y, Su S, Zhang Y, Zhang X,
Giusto P, Huang X and Liu J (2021)
Visible-Light-Driven Photocatalytic
Water Disinfection Toward Escherichia
coli by Nanowired g-C_3N_4 Film.
Front. Nanotechnol. 3:684788.
doi: 10.3389/fnano.2021.684788

Graphitic carbon nitride (g-C_3N_4) as metal-free visible light photocatalyst has recently emerged as a promising candidate for water disinfection. Herein, a nanowire-rich superhydrophilic g-C_3N_4 film was prepared by a vapor-assisted confined deposition method. With a disinfection efficiency of over 99.99% in 4 h under visible light irradiation, this nanowire-rich g-C_3N_4 film was found to perform better than conventional g-C_3N_4 film. Control experiments showed that the disinfection performance of the g-C_3N_4 film reduced significantly after hydrophobic treatment. The potential disinfection mechanism was investigated through scavenger-quenching experiments, which indicate that H_2O_2 was the main active specie and played an important role in bacteria inactivation. Due to the metal-free composition and excellent performance, photocatalytic disinfection by nanowire-rich g-C_3N_4 film would be a promising and cost-effective way for safe drinking water production.

Keywords: superhydrophilic, nanowires, disinfection, photocatalytic, g-C_3N_4 film

INTRODUCTION

The COVID-19 pandemic has demonstrated the critical importance of sanitation, hygiene and adequate access to clean water for preventing and containing diseases. Developing economical and effective water disinfection methods is of great significance for human health as well as alleviating clean water scarcity issues (Xu et al., 2017; Zhang et al., 2018). Conventional water disinfection approaches, including chlorine-based chemical disinfectants, ozone, and ultraviolet (UV), are capable of eliminating a majority of pathogens in water (Xia et al., 2017). However, the disinfection by-products produced by chlorine and chlorine-based disinfectants may cause potential health problems (Li et al., 2017; Huang et al., 2018). Ozone and UV inactivation methods are much safer, but require more energy consumption. Recently, metal-based photocatalysts, such as titanium dioxide (Fernández-Ibáñez et al., 2015; Cavalcante et al., 2016) and zinc oxide (Masoumbaigi et al., 2014), have been extensively investigated as new disinfectants (Cavalcante et al., 2016; Zhang et al., 2018). However, most metal-containing photocatalysts are activated by UV light irradiation, which is only 4% of the solar spectrum reaching earth surface (McGuigan et al., 2012; Ng et al., 2020). Not to mention, secondary pollution may occur due to the inevitable release of metal ions during the disinfection process (Hayden et al., 2010; Bai et al., 2011; Wang et al., 2012; Valsami-Jones and Lynch, 2015; Liu et al., 2016a; Wang and Mi, 2017; Zeng et al.,

2017). Hence, it is of great importance to seek a non-toxic, visible-light-driven and cost-effective method for future water disinfection (Ng et al., 2020).

Due to the metal-free composition, low-cost, suitable bandgap and beneficial energy levels, graphitic carbon nitride (g-C_3N_4) has recently attracted much attention as photocatalyst for water splitting, CO_2 reduction, pollutant degradation, organic syntheses, and bacterial disinfection under visible light irradiation in the past decade (Liu and Antonietti, 2013; Cao et al., 2015; Liu et al., 2015; Liu et al., 2016b; Zhang et al., 2017; Jia et al., 2019; Zhang et al., 2019; Giusto et al., 2020b; Lim et al., 2020; Zhang et al., 2020a; Zhang et al., 2020b). Especially, for bacterial disinfection, most of the previously reported studies focused mainly on the bulk particulate material (Shen et al., 2017; Ran et al., 2019; Gan et al., 2020; Ni et al., 2020; Zhao et al., 2021), which makes recycling difficult and would inevitably lead to secondary pollution of fine nanoparticles (Wang et al., 2019a). Recently, breakthroughs in fabrication methods of g-C_3N_4 films including vapor deposition polymerization, thermal vapor deposition and chemical vapor deposition have led to innovative and inspiring applications in many fields (Thomas et al., 2008; Bian et al., 2015b; Xu et al., 2015a; Xu et al., 2015b; Peng et al., 2018a). It is promising to further improve the performance and stability of g-C_3N_4 materials for water disinfection by employing thin films instead of the common bulk materials (Thomas et al., 2008; Wang et al., 2019c; Chen et al., 2020; Jia et al., 2020; Villalobos et al., 2020). However, the nanoscale topography on such film is usually absent, which would enhance the capture of bacteria from the solution and thereby the disinfection efficiency (Arazoe et al., 2016; Peng et al., 2018b; Jia et al., 2019).

Herein, we report a simple route to synthesize the g-C_3N_4 film featuring numerous nanowires on the top through a vapor-assisted confined deposition onto the ground glass (Bian et al., 2015b; Jia et al., 2019). The adoption of high-roughness ground glass could prevent the easily peeling off of the g-C_3N_4 film, which was usually the case in the smooth counterpart. By adjusting the precursor compositions, the g-C_3N_4 films could be switched from flat surface to nanowired film with superhydrophilic property. Specifically, with the optimal precursor amount and the enhanced vapor pressure at elevated temperature, the formation of nanowire could be expected, which was speculated to be one dimensional growth on the convex bump of the on the flat g-C_3N_4 film (Zhao et al., 2008; Liu et al., 2013). The presence of nanowire on the top of the film could enhance the light harvesting and promote the adhesion of bacterial as well (Liu et al., 2009; Liu et al., 2010). Under visible light irradiation, the nanowire-rich g-C_3N_4 film shows significantly better disinfection performances than the nanowire-free g-C_3N_4 film. By employing the scavenger-quenching experiments, a disinfection mechanism with H_2O_2 as the reactive oxygen species for the g-C_3N_4 film was proposed. A further hydrophobic modification of the pristine nanowire-rich g-C_3N_4 film resulted in diminished disinfection performance, demonstrating the necessity of the beneficial interfacial property. The work reported herein provides a practical and efficient step forward for water disinfection exploiting hierarchical g-C_3N_4 film materials.

EXPERIMENTAL SECTION

All chemicals from commercial sources were used as received without further purification, unless otherwise stated.

A simple vapor-assisted confined deposition method was performed to obtain the nanowire-rich and superhydrophilic g-C_3N_4 films as previously reported (Jia et al., 2019). As shown in **Supplementary Figure S1**, 50 mg of the mixture of melamine and urea (mass ratio of 3:1) was uniformly placed into a ceramic crucible (60 ml) with the cleaned ground glass (2.5 cm × 4 cm) covering the top. Then the entire setup was sealed by aluminum foil. Then the sealed setup was placed in a tubular furnace and maintained at 550°C for 4 h in N_2 atmosphere with a heating rate of 2.3°C/min. The samples were let cool down naturally and collected at room temperature.

The photocatalytic disinfection performance of g-C_3N_4 film was examined by the bacteria inactivation rate of *E. coli* as an indicator. *E. coli* stain was cultured in liquid medium for 18 h, and harvested via centrifuge at 8,000 rpm (5 min). The *E. coli* solution (2 ml, 1×10^4 colony forming unit (CFU) mL^{-1}) was then added to a reactor containing a 10 cm^2 g-C_3N_4 film. A 300 W xenon lamp equipped with a 420 nm cut-off filter (CEL-HXF300, Zhongjiao Jinyuan Technology Co., Ltd. China) was used as a visible light source. Circulating cooling water bath was used to stabilize the temperature of system (25°C). Each batch test lasted for 4 h with samples taken at a 1 h interval. All collected samples were resuspended in phosphate buffer solution and transferred to coated plate. The number of viable cells was determined by plate count method after incubation at 37°C for 18 h. For comparison, control experiments were also conducted in dark condition and in absence of g-C_3N_4. Superhydrophobic samples for control were prepared by modifying the surface of g-C_3N_4 film using polytetrafluoroethylene. For each condition, the experiment was repeated three times. All glass apparatuses and photocatalysts used in the experiments were autoclaved at 121°C for 30 min prior to use and all experiments were operated under sterile conditions.

In order to provide insights on the disinfection mechanism of g-C_3N_4 film, several functional scavengers were added to the system to remove selectively the different active species and depict a preferential disinfection mechanism (Wang et al., 2019b). L-histidine (0.5 mM) was employed for photo-generated singlet oxygen ($^1O_2$) removal, catalase (200 U/mL) for H_2O_2 elimination, sodium oxalate (0.5 mM) for photo-generated holes removal, isopropanol (2.5 mM) for photo-generated OH removal, Cr (VI) (2 mM) for quenching photo-generated electrons, and 4-hydroxy-2,2,6,6-tetramethyl-piperidinyloxy (TEMPOL) (1 mM) to neutralize photo-generated superoxide radicals ($\cdot O_2^-$). The disinfection performance of was tested via cell density quantification. For each condition, the experiment was repeated three times.

The surface morphologies of the as-prepared g-C_3N_4 films were characterized by field-emission scanning electron microscopy (SEM, JSM-7500F). The crystal structure of samples was characterized by X-ray diffraction (XRD) with Cu Kα source radiation (D-MAX 2500/PC diffractometer) in the range from 10 to 50°, with scanning step of 0.02°. The absorption

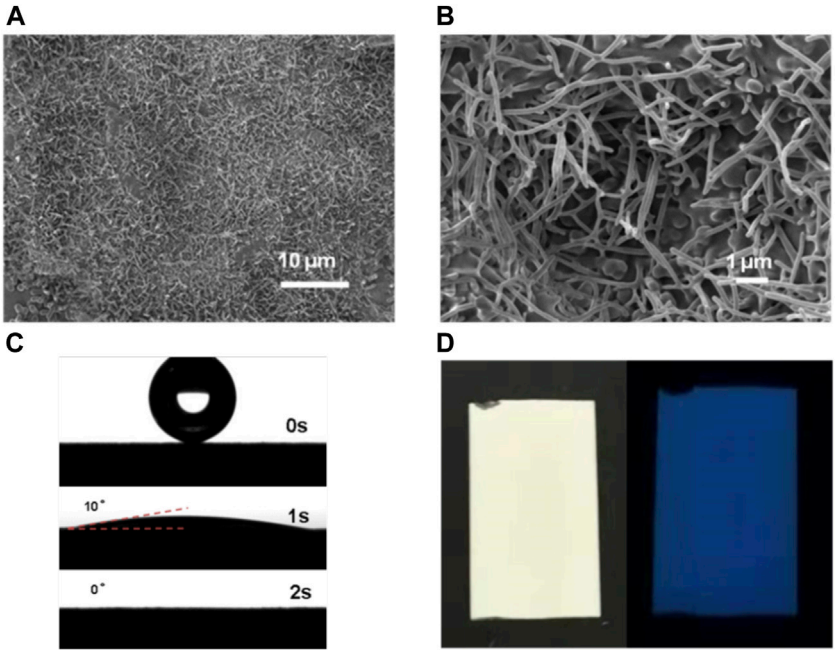

FIGURE 1 | (A, B) SEM images, **(C)** optical contact angle images of water, and **(D)** fluorescence images of g-C_3N_4 film, respectively.

spectra of samples were recorded by UV-vis diffuse reflectance spectra (Hitachi U-3900). Contact angle measurements were performed with a Surface Analyzer (Lauda LSA 60). Visible light irradiation using a 300 W Xenon lamp (CEAULIGHT, Beijing).

RESULTS AND DISCUSSION

Figures 1A,B show the typical SEM images of the obtained g-C_3N_4 films. The nanowires were randomly distributed on the top of the underlayer of the film with the length range about few micrometers. In a typical synthesis of such nanowire-rich g-C_3N_4 film on the ground glass substrate, the mixture of urea and melamine was employed as precursor for thermal polycondensation in a vapor-assisted confined deposition setup. For comparison, either melamine or urea was employed as precursor alone for synthesizing the g-C_3N_4 film and the optical images were shown in **Supplementary Figure S2**. A homogeneous flat film without nanowire formation could be obtained when using either melamine or urea (see SEM images in **Supplementary Figure S3**). This morphology variation could be partly attributed to the formation of a hydrogen-bonded network between melamine and urea during the film growth. Thus, such nanowired thin films could be easily obtained by thermal condensation of melamine and urea mixture in a confined deposition setup (Thomas et al., 2008; Xiong et al., 2020). It's also worth to mention the current method is very economical in terms of the consumed precursor amount, which required only 50 mg of nitrogen-rich precursor to prepare the g-C_3N_4 films over an area of 12.5 m^2 (2.5 cm × 5 cm)(Bian et al., 2015a; Lv et al., 2017; Sheng et al., 2017; Peng et al., 2018b; Lin et al., 2019; Xiao et al., 2019; Giusto et al., 2020b). Previously, only few works report on the wettability of g-C_3N_4 film, which is an important parameter for water disinfection (Liang et al., 2015; Lin et al., 2019; Wu et al., 2019; Giusto et al., 2020c). As displayed in **Figure 1C**, the water wettability on such film was investigated by contact angel measurements. The as-prepared g-C_3N_4 films are proven to be superhydrophilic. When a water droplet (2 μL) was deposited on the film, it quickly spread on the surface. Finally, the droplet spread out completely and the contact angle decreased to 0° within 2 s. So, the g-C_3N_4 film prepared by this method exhibits superhydrophilicity, which is conducive to improving disinfection performance. As shown, the as-prepared films present the typical bright yellow color of g-C_3N_4, with an intense blue homogeneous fluorescence when irradiated with UV light, confirming that the deposition occurred homogeneously over the whole substrate surface (**Figure 1D**). The optical properties of the as-prepared g-C_3N_4 films were further studied by photoluminescence (PL) at an excitation wavelength of 365 nm (**Supplementary Figure S4**). In addition to the film prepared by urea, the other g-C_3N_4 films showed a strong PL emission centered at about 466 nm, which is corresponding to the absorption edges in UV-vis diffuse reflectance spectra. And the emission intensity of g-C_3N_4 film prepared by the mixture of melamine and urea is stronger than the g-C_3N_4 film prepared by melamine alone, indicating the low charge separation efficiency of photogenerated electron-hole pairs of the former.

The UV–Vis diffuse reflectance absorbance spectra of the bulk g-C_3N_4 and g-C_3N_4 film are shown in **Figure 2A**.

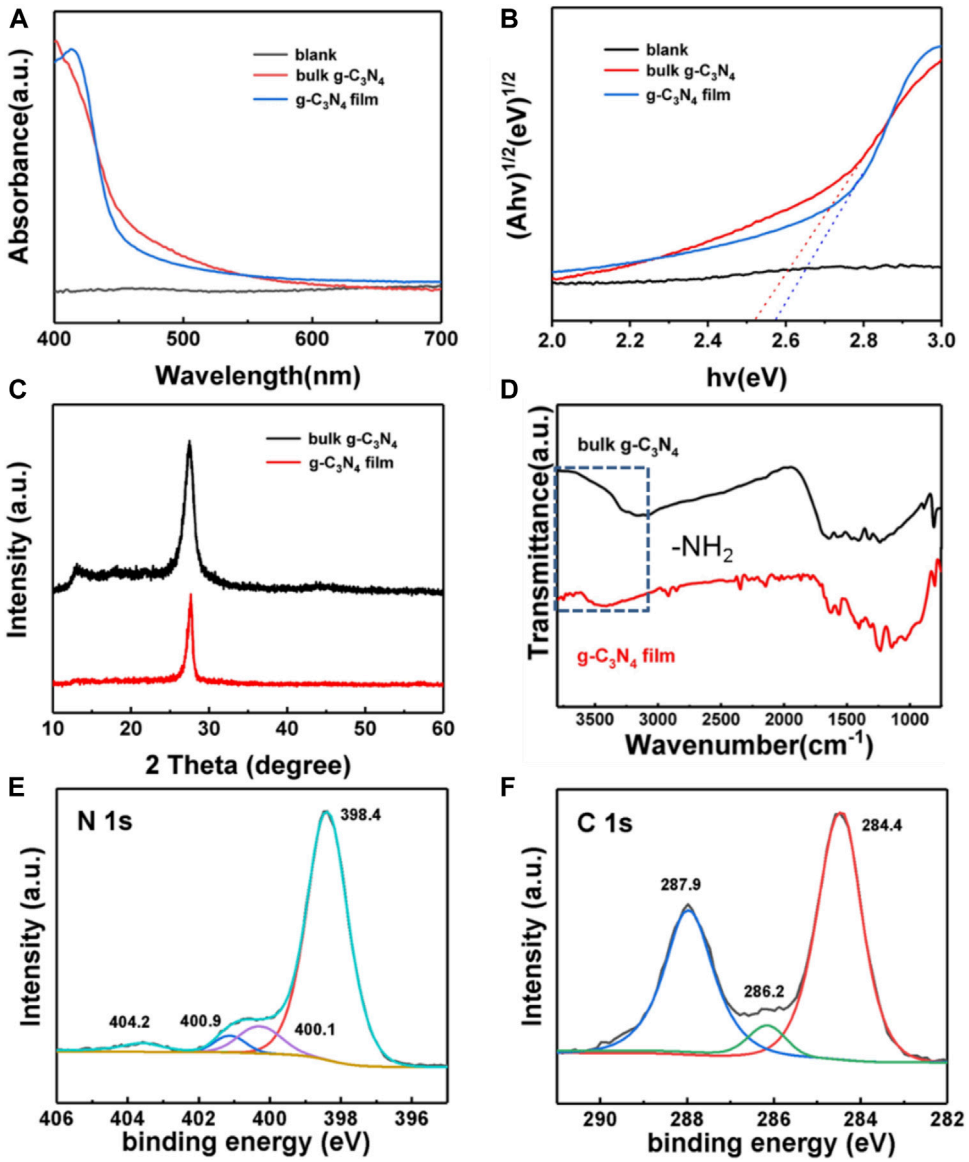

FIGURE 2 | (A) UV–Vis absorption spectra of blank glass (black line), bulk g-C_3N_4 (red line) and g-C_3N_4 film (blue line), respectively. **(B)** Tauc plots of blank glass (black line), bulk g-C_3N_4 (red line) and g-C_3N_4 film (blue line), respectively. **(C)** XRD diffraction patterns of bulk g-C_3N_4 (black line) and g-C_3N_4 film (red line). **(D)** Infrared spectra of bulk g-C_3N_4 (black line) and g-C_3N_4 film (red line). **(E)** Typical N 1s and **(F)** C 1s XPS spectra of g-C_3N_4 film.

The bulk and the nanowired film show similar optical properties with their absorption edges locating at 471 and 456 nm, respectively. Correspondingly, their optical band gaps are 2.52 and 2.58 eV as identified by the Kubelka-Munk method (**Figure 2B**), which is in good agreement with previous reports (Giusto et al., 2020a). At the same time, we measured the transmittance of these three kinds of g-C_3N_4 films, and found that the g-C_3N_4 film prepared by the mixture of melamine and urea is more opaque, which will be more conducive to light absorption (**Supplementary Figure S5**).

The crystallinity of the g-C_3N_4 film and powder were analyzed by XRD and the corresponding results are shown in **Figure 2C**. The diffraction peaks of bulk powder with strong intensity located at 27.5° and 13.1° could be ascribed to the typical graphitic interlayer (002) plane and the in-plane structural repeating unit of the aromatic systems, respectively (Thomas et al., 2008). The g-C_3N_4 film shows a peak at 27° while the peak of (100) plan disappeared. Due to the enhanced roughness of the ground glass, the obtained film could not be easily peeled off from the substrate. So we have to prepare a lot of g-C_3N_4 film to scrape the powder for the measure. For comparison purpose, nearly all the g-C_3N_4 film grown on the smooth glass surface could be easily peeled off from the substrate and could get wrinkled and crushed to particles in a sustained reaction under aqueous environment (Arazoe et al., 2016; Xiao et al., 2018; Jia et al., 2019).

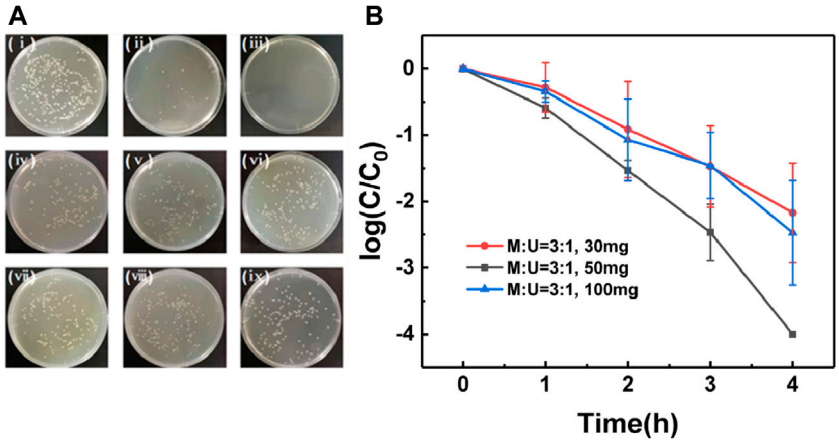

FIGURE 3 | (A) Photos of *E. coli* on plate count agars spread before and after photocatalytic disinfection using g-C_3N_4 film: under visible light irradiation for (i) 0 h (ii) 2 h and (iii) 4 h. Photos of *E. coli* on an agar plate before and after photocatalytic disinfection without g-C_3N_4 film: under visible light irradiation for (iv) 0 h (v) 2 h and (vi) 4 h. Photos of *E. coli* on an agar plate before and after photocatalytic disinfection without visible light irradiation (vii) 0 h, (viii) 2 h and (ix) 4 h. **(B)** Comparison of the disinfection performance of g-C_3N_4 film with control experiments.

The typical features of g-C_3N_4 materials can be depicted by means of Fourier transform infrared spectroscopy (FTIR) (**Figure 2D**). The peak at 807 cm^{-1} corresponds to the out-of plane ring bending of the triazine unit with the characteristic stretching modes of the CN heterocycles was observed ranging from 1,040 to 1,640 cm^{-1}. And the broad absorption peak from 2,900 to 3,600 cm^{-1} is attributed to the stretching vibration of terminal -NH_2 group.

XPS spectra of the film give more insights on its chemical features (**Figure 2E**). The N 1s spectrum can be deconvoluted into four peaks corresponding to nitrogen atoms in different functional groups: sp (Xu et al., 2017) hybridized aromatic N bonded to carbon atoms of the s-triazine ring at 398.4 eV, tertiary N bonded to carbon atoms in the form of N-$(C)_3$ at 400.1 eV, amino functional groups with hydrogen (C–N–H) at 400.9 eV, and π-excitations at 404.2 eV. Three fitting peaks located at 284.4, 286.2, and 287.9 eV in **Figure 2F** corresponded to the graphitic carbon (C–C), the sp (Xu et al., 2017)-type C=N bonds and sp (Xu et al., 2017) hybridized carbon in tri-*s*-triazine rings (N_2-C=N), respectively. The XPS spectra demonstrate the presence of the tri-s-triazine units, which is in good agreement with FTIR spectra.

In this work, *E. coli*, one of the most commonly available bacteria, was selected as a model microbe to evaluate the deactivation performances. The photocatalytic disinfection performances can be clearly seen even by naked eyes in the digital images from the agar plates containing the bacterial culture of *E. coli* collected at 0-, 2- and 4-hours steps (**Figures 3A,I, ii,iii** are 0, 2 and 4 h respectively), while no difference can be seen in absence of the photocatalyst or visible light (**Figure 3A iv–ix**). The high disinfection efficiency and the synergistic effect of g-C_3N_4 and visible light is confirmed with the residual bacteria counting (**Figure 3B**): indeed, most of the *E. coli* was inactivated already in 2 h, and almost complete inactivation (>99.99%) was reached after 4 h. Negligible variation of the bacteria activities was obtained in the reference cases (<1%), using only the g-C_3N_4 film in dark (**Figure 3B**, blue line) or in absence of the photocatalyst (**Figure 3B**, red line). The obtained results confirms unequivocally that high disinfection performances are obtained only by the synergistic effect of g-C_3N_4 and visible light. It is worth mentioning that the g-C_3N_4 film is still strongly bonded to the substrate after the sterilization experiment, which provides the possibility for the subsequent repeated experiments (**Supplementary Figure S6**). The stability of g-C_3N_4 membrane was investigated by repeating *E. coli* inactivation experiments with recycled g-C_3N_4 membrane. After three times' recycling, disinfection performance of g-C_3N_4 film has not decreased significantly (**Supplementary Figure S7**).

We further investigated the effect of the precursor mass on the disinfection performances. As shown in the following (**Figure 4A**), the optimum of disinfection was achieved by using 50 mg of precursor, with respect to 30 and 100 mg. It is worth noting that by using 50 mg precursor, the resulting g-C_3N_4 film showed a higher density of nanowires per unit area, which resulted in a better disinfection activity compared to the other two cases, as confirmed by SEM (**Supplementary Figure S8**). Therefore, we attributed the enhanced disinfection ability to the nanowired structure which allows for an intimate contact between the g-C_3N_4 film and the bacterial disinfection with efficient separation of electrons and holes. The influence of nanowires on the disinfection performance was investigated in an experiment by using different precursor. The results showed that the g-C_3N_4 film with nanowired structure has a better disinfection performance (**Supplementary Figure S9**). Since the *E. coli* concentration after 4 h was almost four order of magnitude lower, we further investigated on the performances of the film prepared from 50 mg precursor.

To further prove that the surface wettability influences the effective contact between the photocatalyst and bacteria, the hydrophilic g-C_3N_4 film was treated with

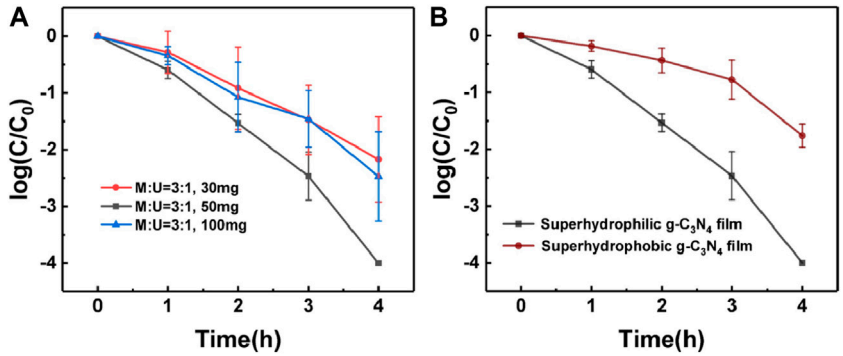

FIGURE 4 | (A) Effect of precursor mass on disinfection performance of g-C_3N_4 film. **(B)** Effect of wettability on photocatalytic disinfection.

polytetrafluorethylene to increase surface hydrophobicity (**Supplementary Figure S10**) and study how that influences the performances (Sheng et al., 2017). The effect of hydrophobic treatment on photocatalytic disinfection was investigated over time and compared to the bare sample (**Figure 4B**), confirming that the superhydrophilic properties are of paramount importance for improving the disinfection process. Superhydrophilicity guarantees the close contact between bacteria and photocatalyst, which leads to the quite high catalytic activity.

During the photocatalytic disinfection, active species, such as H_2O_2, e^-, $^{\cdot}OH$, $^{\cdot}O_2^-$, $^1O_2$ and h^+, are directly involved in the disinfection step, as shown in **Scheme 1** (Liang et al., 2015). In order to study the mechanism of g-C_3N_4 film, we performed further tests using selective scavengers. Several scavengers were added to the solution containing *E. coli* to eliminate the corresponding active species, and the photocatalytic reaction without scavenger was used as the control group (**Figure 5**).

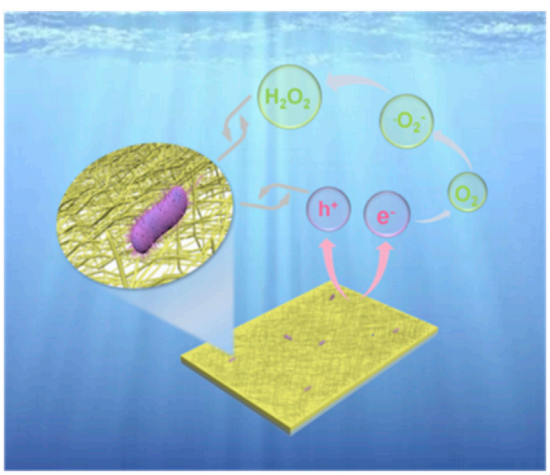

SCHEME 1 | The proposed disinfection mechanism of nanowire-rich g-C_3N_4 film.

The addition of L-histidine exhibited negligible influence on the disinfection performance (**Figure 5A**). Addition of catalase significantly reduced the photocatalytic disinfection efficiency, suggesting that H_2O_2 play an important role in bacterial inactivation (**Figure 5B**). The photo-generated holes were much less likely to come into direct contact with bacteria. Moreover, h^+ is more difficult to diffuse than H_2O_2, and the photo-generated lifetime is also extremely short. Therefore, H_2O_2 served as the disinfectant has a more important role than h^+ (**Figure 5C**). The valence band position of g-C_3N_4 is more negative than the redox potential of OH/OH^-, it is difficult for OH^- to be oxidized to generate OH. Thus, the role of OH in the photocatalytic disinfection is only minor (**Figure 5D**). As reported, $\cdot O_2^-$ and e^- were also critical active species in the photocatalytic disinfection process (Xu et al., 2017; Liang et al., 2015), because the photocatalytic disinfection could occur through oxidation by active oxidants and reduction by electrons (**Figure 5E**). Indeed, the addition of TEMPOL reduces significantly the photocatalytic efficiency (**Figure 5F**). As the superoxide anion ($\cdot O_2^-$) is an active intermediate in the production of H_2O_2, the more O_2^- is produced, the more H_2O_2 will be generated. Based on these results we can then confirm that the disinfection mechanism occurs via the generation of superoxide and water peroxide, and thus is related to the strong oxidation properties of g-C_3N_4 (Mazzanti and Savateev, 2020).

CONCLUSION

In this work, a superhydrophilic nanowire-rich g-C_3N_4 film was synthesized and applied for disinfection to remove *E. coli* under visible light irradiation. The disinfection efficiency could reach over 99.99% in 4 h under visible light irradiation when the mass of the precursor was 50 mg. Surface wettability investigation demonstrated that the superhydrophilic property enhances the photocatalytic disinfection performance greatly, while hydrophobic treatments to the surface lead to an increase of the contact angle and a decrease of the disinfection. Mechanism for disinfection was further explored with H_2O_2 being the crucial active specie. Furthermore, the convenient use of the g-C_3N_4 as a surface-immobilized film allows

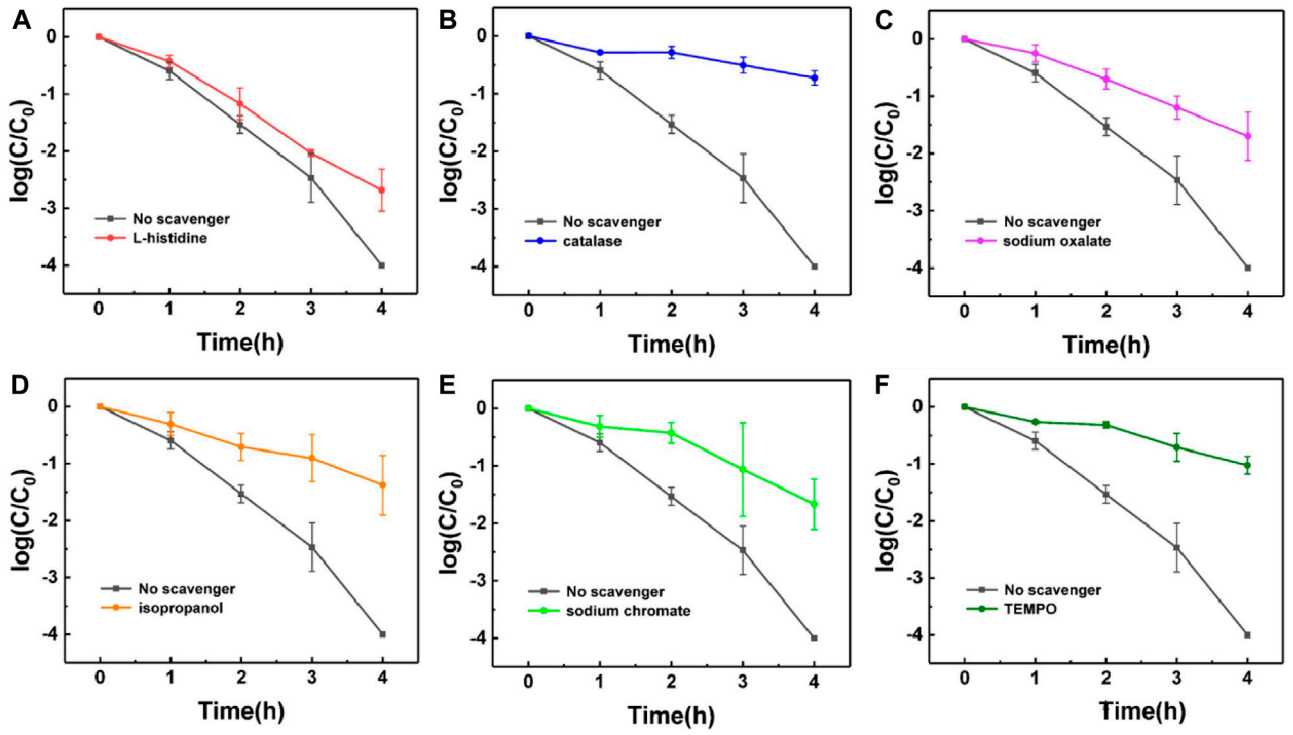

FIGURE 5 | Photochemical analysis of disinfection mechanism via addition of various scavengers using L-histidine **(A)**, catalase **(B)**, sodium oxalate **(C)**, isopropanol **(D)**, Cr (VI) **(E)** and TEMPOL **(F)** as scavenger respectively. In these disinfection performance curves, error bars represent the standard deviation of three replicate measurements.

for simple and complete removal of the photocatalyst after the disinfection process. We expect therefore that these results will encourage further investigation and development of metal-free carbon materials for water disinfection applications.

DATA AVAILABILITY STATEMENT

The original contributions presented in the study are included in the article/**Supplementary Material**, further inquiries can be directed to the corresponding authors.

AUTHOR CONTRIBUTIONS

JL conceived the idea. YZ and SS performed the experiments and drafted the manuscript. YZ, XZ, PG, XH, contributed to the discussion of the experimental data and the writing of the manuscript. PG, XH, JL contributed to the writing, reviewing and editing of the manuscript. JL contributed to the funding acquisition and supervised the project.

FUNDING

This work was financially supported by the Natural Science Foundation of Shandong Province (ZR2018MB018).

SUPPLEMENTARY MATERIAL

The Supplementary Material for this article can be found online at: https://www.frontiersin.org/articles/10.3389/fnano.2021.684788/full#supplementary-material

REFERENCES

Arazoe, H., Miyajima, D., Akaike, K., Araoka, F., Sato, E., Hikima, T., et al. (2016). An Autonomous Actuator Driven by Fluctuations in Ambient Humidity. *Nat. Mater* 15 (10), 1084–1089. doi:10.1038/nmat4693

Bai, H., Liu, Z., and Sun, D. D. (2011). Hierarchical ZnO/Cu "Corn-like" Materials with High Photodegradation and Antibacterial Capability under Visible Light. *Phys. Chem. Chem. Phys.* 13, 6205–6210. doi:10.1039/c0cp02546a

Bian, J., Li, J., Kalytchuk, S., Wang, Y., Li, Q., Lau, T. C., et al. (2015a). Efficient Emission Facilitated by Multiple Energy Level Transitions in Uniform Graphitic Carbon Nitride Films Deposited by Thermal Vapor Condensation. *Chemphyschem* 16, 954–959. doi:10.1002/cphc.201402898

Bian, J., Li, Q., Huang, C., Li, J., Guo, Y., Zaw, M., et al. (2015b). Thermal Vapor Condensation of Uniform Graphitic Carbon Nitride Films with Remarkable Photocurrent Density for Photoelectrochemical Applications. *Nano Energy* 15, 353–361. doi:10.1016/j.nanoen.2015.04.012

Cao, S., Low, J., Yu, J., and Jaroniec, M. (2015). Polymeric Photocatalysts Based on Graphitic Carbon Nitride. *Adv. Mater.* 27, 2150–2176. doi:10.1002/adma.201500033

Cavalcante, R. P., Dantas, R. F., Bayarri, B., González, O., Giménez, J., Esplugas, S., et al. (2016). Photocatalytic Mechanism of Metoprolol Oxidation by Photocatalysts TiO_2 and TiO_2 Doped with 5% B: Primary Active Species and Intermediates. *Appl. Catal. B* 194, 111–122. doi:10.1016/j.apcatb.2016.04.054

Chen, L., Yan, R., Oschatz, M., Jiang, L., Antonietti, M., and Xiao, K. (2020). Ultrathin 2D Graphitic Carbon Nitride on Metal Films: Underpotential Sodium Deposition in Adlayers for Sodium-Ion Batteries. *Angew. Chem. Int. Ed.* 59, 9067–9073. doi:10.1002/anie.202000314

Fernández-Ibáñez, P., Polo-López, M. I., Malato, S., Wadhwa, S., Hamilton, J. W. J., Dunlop, P. S. M., et al. (2015). Solar Photocatalytic Disinfection of Water Using Titanium Dioxide Graphene Composites. *Chem. Eng. J.* 261, 36–44. doi:10.1016/j.cej.2014.06.089

Gan, Z., Huang, C., Shen, Y., Zhou, Q., Han, D., Ma, J., et al. (2020). Preparation of Carbon Nitride Nanoparticles by Nanoprecipitation Method with High Yield and Enhanced Photocatalytic Activity. *Chin. Chem. Lett.* 31, 513–516. doi:10.1016/j.cclet.2019.04.065

Giusto, P., Arazoe, H., Cruz, D., Lova, P., Heil, T., Aida, T., et al. (2020a). Boron Carbon Nitride Thin Films: From Disordered to Ordered Conjugated Ternary Materials. *J. Am. Chem. Soc.* 142, 20883–20891. doi:10.1021/jacs.0c10945

Giusto, P., Cruz, D., Heil, T., Arazoe, H., Lova, P., Aida, T., et al. (2020b). Shine Bright like a Diamond: New Light on an Old Polymeric Semiconductor. *Adv. Mater.* 32, e1908140. doi:10.1002/adma.201908140

Giusto, P., Kumru, B., Zhang, J., Rothe, R., and Antonietti, M. (2020c). Let a Hundred Polymers Bloom: Tunable Wetting of Photografted Polymer-Carbon Nitride Surfaces. *Chem. Mater.* 32, 7284–7291. doi:10.1021/acs.chemmater.0c01798

Hayden, S. C., Allam, N. K., and El-Sayed, M. A. (2010). TiO_2 Nanotube/CdS Hybrid Electrodes: Extraordinary Enhancement in the Inactivation of *Escherichia Coli*. *J. Am. Chem. Soc.* 132, 14406–14408. doi:10.1021/ja107034z

Huang, Y., Li, H., Zhou, Q., Li, A., Shuang, C., Xian, Q., et al. (2018). New Phenolic Halogenated Disinfection Byproducts in Simulated Chlorinated Drinking Water: Identification, Decomposition, and Control by Ozone-Activated Carbon Treatment. *Water Res.* 146, 298–306. doi:10.1016/j.watres.2018.09.031

Jia, C., Hu, W., Zhang, Y., Teng, C., Chen, Z., and Liu, J. (2020). Facile Assembly of a Graphitic Carbon Nitride Film at an Air/water Interface for Photoelectrochemical NADH Regeneration. *Inorg. Chem. Front.* 7, 2434–2442. doi:10.1039/d0qi00182a

Jia, F., Zhang, Y., Hu, W., Lv, M., Jia, C., and Liu, J. (2019). *In-Situ* Construction of Superhydrophilic G-C_3n_4 Film by Vapor-Assisted Confined Deposition for Photocatalysis. *Front. Mater.* 6, 52. doi:10.3389/fmats.2019.00052

Li, C., Wang, D., Xu, X., and Wang, Z. (2017). Formation of Known and Unknown Disinfection By-Products from Natural Organic Matter Fractions during Chlorination, Chloramination, and Ozonation. *Sci. Total Environ.* 587-588, 177–184. doi:10.1016/j.scitotenv.2017.02.108

Liang, J., Shan, C., Zhang, X., and Tong, M. (2015). Bactericidal Mechanism of BiOI-AgI under Visible Light Irradiation. *Chem. Eng. J.* 279, 277–285. doi:10.1016/j.cej.2015.05.024

Lim, J., Kim, H., Park, J., Moon, G. H., Vequizo, J. J. M., Yamakata, A., et al. (2020). How g-C_3N_4 Works and Is Different from TiO_2 as an Environmental Photocatalyst: Mechanistic View. *Environ. Sci. Technol.* 54, 497–506. doi:10.1021/acs.est.9b05044

Lin, B., Yang, G., and Wang, L. (2019). Stacking-Layer-Number Dependence of Water Adsorption in 3D Ordered Close-Packed g-C_3N_4 Nanosphere Arrays for Photocatalytic Hydrogen Evolution. *Angew. Chem. Int. Ed.* 58, 4587–4591. doi:10.1002/anie.201814360

Liu, C., Kong, D., Hsu, P.-C., Yuan, H., Lee, H.-W., Liu, Y., et al. (2016a). Rapid Water Disinfection Using Vertically Aligned MoS2 Nanofilms and Visible Light. *Nat. Nanotech* 11, 1098–1104. doi:10.1038/nnano.2016.138

Liu, J., and Antonietti, M. (2013). Bio-inspired NADH Regeneration by Carbon Nitride Photocatalysis Using Diatom Templates. *Energy Environ. Sci.* 6, 1486–1493. doi:10.1039/c3ee40696b

Liu, J., Huang, J., Dontosova, D., and Antonietti, M. (2013). Facile Synthesis of Carbon Nitride Micro-/Nanoclusters with Photocatalytic Activity for Hydrogen Evolution. *RSC Adv.* 3, 22988–22993. doi:10.1039/c3ra44490b

Liu, J., Li, M., Wang, J., Song, Y., Jiang, L., Murakami, T., et al. (2009). Hierarchically Macro-/Mesoporous Ti–Si Oxides Photonic Crystal with Highly Efficient Photocatalytic Capability. *Environ. Sci. Technol.* 43 (24), 9425–9431. doi:10.1021/es902462c

Liu, J., Liu, G., Li, M., Shen, W., Liu, Z., Wang, J., et al. (2010). Enhancement of Photochemical Hydrogen Evolution over Pt-Loaded Hierarchical Titania Photonic Crystal. *Energ. Environ. Sci.* 3 (10), 1503–1506. doi:10.1039/c0ee00116c

Liu, J., Wang, H., and Antonietti, M. (2016b). Graphitic Carbon Nitride "Reloaded": Emerging Applications beyond (Photo)Catalysis. *Chem. Soc. Rev.* 45, 2308–2326. doi:10.1039/c5cs00767d

Liu, J., Wang, H., Chen, Z. P., Moehwald, H., Fiechter, S., van de Krol, R., et al. (2015). Microcontact-Printing-Assisted Access of Graphitic Carbon Nitride Films with Favorable Textures toward Photoelectrochemical Application. *Adv. Mater.* 27, 712–718. doi:10.1002/adma.201404543

Lv, X., Cao, M., Shi, W., Wang, M., and Shen, Y. (2017). A New Strategy of Preparing Uniform Graphitic Carbon Nitride Films for Photoelectrochemical Application. *Carbon* 117, 343–350. doi:10.1016/j.carbon.2017.02.096

Masoumbaigi, H., Rezaee, A., Hosseini, H., and Hashemi, S. (2014). Water Disinfection by Zinc Oxide Nanoparticle Prepared with Solution Combustion Method. *Desalination Water Treat.* 56, 2376–2381. doi:10.1080/19443994.2014.961556

Mazzanti, S., and Savateev, A. (2020). Emerging Concepts in Carbon Nitride Organic Photocatalysis. *ChemPlusChem* 85, 2499–2517. doi:10.1002/cplu.202000606

McGuigan, K. G., Conroy, R. M., Mosler, H.-J., Preez, M. d., Ubomba-Jaswa, E., and Fernandez-Ibañez, P. (2012). Solar Water Disinfection (SODIS): A Review from Bench-Top to Roof-Top. *J. Hazard. Mater.* 235-236, 29–46. doi:10.1016/j.jhazmat.2012.07.053

Ng, B. J., Musyaffa, M. K., Er, C. C., Packiam, K. A. R., Lee, W. P. C., Tan, L. L., et al. (2020). Proton-Functionalized Graphitic Carbon Nitride for Efficient Metal-free Disinfection of Escherichia Coli under Low-Power Light Irradiation. *Chemistry* 4, 5822. doi:10.1002/chem.202004238

Ni, D., Zhang, Y., Shen, Y., Liu, S., and Zhang, Y. (2020). Promoting Condensation Kinetics of Polymeric Carbon Nitride for Enhanced Photocatalytic Activities. *Chin. Chem. Lett.* 31, 115–118. doi:10.1016/j.cclet.2019.04.068

Peng, G., Albero, J., Garcia, H., and Shalom, M. (2018a). A Water-Splitting Carbon Nitride Photoelectrochemical Cell with Efficient Charge Separation and Remarkably Low Onset Potential. *Angew. Chem. Int. Ed.* 57, 15807–15811. doi:10.1002/anie.201810225

Peng, G., Xing, L., Barrio, J., Volokh, M., and Shalom, M. (2018b). A General Synthesis of Porous Carbon Nitride Films with Tunable Surface Area and Photophysical Properties. *Angew. Chem. Int. Ed.* 57, 1186–1192. doi:10.1002/anie.201711669

Ran, M., Chen, P., Li, J., Cui, W., Li, J., He, Y., et al. (2019). Promoted Reactants Activation and Charge Separation Leading to Efficient Photocatalytic Activity on Phosphate/potassium Co-functionalized Carbon Nitride. *Chin. Chem. Lett.* 30, 875–880. doi:10.1016/j.cclet.2019.03.016

Shen, Y.-F., Zhang, C., Yan, C.-G., Chen, H.-Q., and Zhang, Y.-J. (2017). Fabrication of Porous Graphitic Carbon Nitride-Titanium Dioxide Heterojunctions with Enhanced Photo-Energy Conversion Activity. *Chin. Chem. Lett.* 28, 1312–1317. doi:10.1016/j.cclet.2017.04.004

Sheng, X., Liu, Z., Zeng, R., Chen, L., Feng, X., and Jiang, L. (2017). Enhanced Photocatalytic Reaction at Air-Liquid-Solid Joint Interfaces. *J. Am. Chem. Soc.* 139, 12402–12405. doi:10.1021/jacs.7b07187

Thomas, A., Fischer, A., Goettmann, F., Antonietti, M., Müller, J.-O., Schlögl, R., et al. (2008). Graphitic Carbon Nitride Materials: Variation of Structure and Morphology and Their Use as Metal-free Catalysts. *J. Mater. Chem.* 18, 4893–4908. doi:10.1039/b800274f

Valsami-Jones, E., and Lynch, I. (2015). How Safe Are Nanomaterials?. *Science* 350, 388–389. doi:10.1126/science.aad0768

Villalobos, L. F., Vahdat, M. T., Dakhchoune, M., Nadizadeh, Z., Mensi, M., Oveisi, E., et al. (2020). Large-Scale Synthesis of Crystalline G-C_3n_4 Nanosheets and High-Temperature H_2 Sieving from Assembled Films. *Sci. Adv.* 6, eaay9851. doi:10.1126/sciadv.aay9851

Wang, L., Tong, Y., Feng, J., Hou, J., Li, J., Hou, X., et al. (2019a). A Rising Star for Photoelectrochemical Water Splitting, g-C_3N_4-based films. *Sustain. Mater. Technol.* 19, e00089. doi:10.1016/j.susmat.2018.e00089

Wang, L., Tong, Y., Feng, J., Hou, J., Li, J., Hou, X., et al. (2019b). G-C_3N_4-based Films: A Rising Star for Photoelectrochemical Water Splitting. *SM&T* 19, e0089. doi:10.1016/j.susmat.2018.e00089

Wang, W., Yu, Y., An, T., Li, G., Yip, H. Y., Yu, J. C., et al. (2012). Visible-Light-Driven Photocatalytic Inactivation of E. coli K-12 by Bismuth Vanadate Nanotubes: Bactericidal Performance and Mechanism. *Environ. Sci. Technol.* 46, 4599–4606. doi:10.1021/es2042977

Wang, Y., Wu, N., Wang, Y., Ma, H., Zhang, J., Xu, L., et al. (2019c). Graphite Phase Carbon Nitride Based Membrane for Selective Permeation. *Nat. Commun.* 10, 2500. doi:10.1038/s41467-019-10381-z

Wang, Z., and Mi, B. (2017). Environmental Applications of 2D Molybdenum Disulfide (MoS2) Nanosheets. *Environ. Sci. Technol.* 51, 8229–8244. doi:10.1021/acs.est.7b01466

Wu, Y., Feng, J., Gao, H., Feng, X., and Jiang, L. (2019). Superwettability-Based Interfacial Chemical Reactions. *Adv. Mater.* 31, e1800718. doi:10.1002/adma.201800718

Xia, D., Li, Y., Huang, G., Yin, R., An, T., Li, G., et al. (2017). Activation of Persulfates by Natural Magnetic Pyrrhotite for Water Disinfection: Efficiency, Mechanisms, and Stability. *Water Res.* 112, 236–247. doi:10.1016/j.watres.2017.01.052

Xiao, K., Chen, L., Chen, R., Heil, T., Lemus, S. D. C., Fan, F., et al. (2019). Artificial Light-Driven Ion Pump for Photoelectric Energy Conversion. *Nat. Commun.* 10, 74. doi:10.1038/s41467-018-08029-5

Xiao, K., Giusto, P., Wen, L., Jiang, L., and Antonietti, M. (2018). Nanofluidic Ion Transport and Energy Conversion through Ultrathin Free-Standing Polymeric Carbon Nitride Membranes. *Angew. Chem. Int. Ed.* 57, 10123–10126. doi:10.1002/anie.201804299

Xiong, W., Huang, F., and Zhang, R.-Q. (2020). Recent Developments in Carbon Nitride Based Films for Photoelectrochemical Water Splitting. *Sustain. Energ. Fuels* 4, 485–503. doi:10.1039/c9se00785g

Xu, J., Herraiz-Cardona, I., Yang, X., Gimenez, S., Antonietti, M., and Shalom, M. (2015a). The Complex Role of Carbon Nitride as a Sensitizer in Photoelectrochemical Cells. *Adv. Opt. Mater.* 3, 1052–1058. doi:10.1002/adom.201500010

Xu, J., Shalom, M., Piersimoni, F., Antonietti, M., Neher, D., and Brenner, T. J. K. (2015b). Color-Tunable Photoluminescence and NIR Electroluminescence in Carbon Nitride Thin Films and Light-Emitting Diodes. *Adv. Opt. Mater.* 3, 913–917. doi:10.1002/adom.201500019

Xu, J., Wang, Z., and Zhu, Y. (2017). Enhanced Visible-Light-Driven Photocatalytic Disinfection Performance and Organic Pollutant Degradation Activity of Porous G-C3n4 Nanosheets. *ACS Appl. Mater. Inter.* 9, 27727–27735. doi:10.1021/acsami.7b07657

Zeng, X., Wang, Z., Wang, G., Gengenbach, T. R., McCarthy, D. T., Deletic, A., et al. (2017). Highly Dispersed TiO2 Nanocrystals and WO3 Nanorods on Reduced Graphene Oxide: Z-Scheme Photocatalysis System for Accelerated Photocatalytic Water Disinfection. *Appl. Catal. B: Environ.* 218, 163–173. doi:10.1016/j.apcatb.2017.06.055

Zhang, B., Zou, S., Cai, R., Li, M., and He, Z. (2018). Highly-Efficient Photocatalytic Disinfection of Escherichia Coli under Visible Light Using Carbon Supported Vanadium Tetrasulfide Nanocomposites. *Appl. Catal. B: Environ.* 224, 383–393. doi:10.1016/j.apcatb.2017.10.065

Zhang, C., Li, Y., Shuai, D., Shen, Y., Xiong, W., and Wang, L. (2019). Graphitic Carbon Nitride (G-C3n4)-Based Photocatalysts for Water Disinfection and Microbial Control: A Review. *Chemosphere* 214, 462–479. doi:10.1016/j.chemosphere.2018.09.137

Zhang, W., Albero, J., Xi, L., Lange, K. M., Garcia, H., Wang, X., et al. (2017). One-Pot Synthesis of Nickel-Modified Carbon Nitride Layers toward Efficient Photoelectrochemical Cells. *ACS Appl. Mater. Inter.* 9, 32667–32677. doi:10.1021/acsami.7b08022

Zhang, Y., Huang, X., Li, J., Lin, G., Liu, W., Chen, Z., et al. (2020a). Iron-doping Accelerating NADH Oxidation over Carbon Nitride. *Chem. Res. Chin. Univ.* 36, 1076–1082. doi:10.1007/s40242-020-0293-x

Zhang, Y., Zhao, Y., Li, R., and Liu, J. (2020b). Bioinspired NADH Regeneration Based on Conjugated Photocatalytic Systems. *Sol. RRL* 5, 2000339. doi:10.1002/solr.202000339

Zhao, G., Xing, Y., Hao, S., Xu, X., Ma, W., and Guo, J. (2021). Why the Hydrothermal Fluorinated Method Can Improve Photocatalytic Activity of Carbon Nitride. *Chin. Chem. Lett.* 32, 277–281. doi:10.1016/j.cclet.2020.11.033

Zhao, Y., Liu, Z., Chu, W., Song, L., Zhang, Z., Yu, D., et al. (2008). Large-Scale Synthesis of Nitrogen-Rich Carbon Nitride Microfibers by Using Graphitic Carbon Nitride as Precursor. *Adv. Mater.* 20, 1777–1781. doi:10.1002/adma.200702230

Conflict of Interest: Author XH was employed by company Bestee Materials (Tsingdao) Co. Ltd.

The remaining authors declare that the research was conducted in the absence of any commercial or financial relationships that could be construed as a potential conflict of interest.

The reviewer KX declared a past co-authorship with one of the authors PG to the handling Editor.